Scientific Research Publishing

Advances in Pure Mathematics, 2020, 10, 471-491
https://www.scirp.org/journal/apm
ISSN Online: 2160-0384
ISSN Print: 2160-0368

Monte Carlo Simulations of Topological Properties in Two-Phase Polycrystalline Materials for Several Diffusion Mechanisms

Rifa J. El-Khozondar

Physics Department, Al-Aqsa University, Gaza, Palestine
Email: rifa20012002@yahoo.com

How to cite this paper: El-Khozondar, R.J. (2020) Monte Carlo Simulations of Topological Properties in Two-Phase Polycrystalline Materials for Several Diffusion Mechanisms. *Advances in Pure Mathematics*, **10**, 471-491.
https://doi.org/10.4236/apm.2020.109029

Received: July 13, 2020
Accepted: September 5, 2020
Published: September 8, 2020

Abstract

Numerical simulations by means of the Monte Carlo Potts model have been provided to simulate grain structures in two-phase polycrystalline materials. The topological features in the simulated microstructure analyzed for different diffusion mechanisms over a broad range of volume fractions for both phases. The topological properties include the average number of sides, grain topology distribution and the topological size relation function. It is found that the average number of sides depends proportionally on the volume fraction. It increases as the volumes fraction increases and vice versa. Moreover, it is shown that the grain topology distribution in the self-similar growth regime can be described by time unchanged function of the relative grain size. Additionally, topological size function in the simulated microstructure can be evaluated by a quadratic function.

Keywords

Monte Carlo Potts Model, Topology Distribution, Polycrystalline, Microstructure, Diffusion Mechanisms

1. Introduction

In one-phase systems, grain growth is motivated by lessening in the entire interfacial energy. The velocity of grain boundaries is measured by the rate of atom removal across the boundary. Consequently, the diffusion distance of atoms is nearly equivalent to the width of the grain boundary.

In two-phase systems, the grain structure evolves by Ostwald ripening. Ostwald ripening may occur by two variant processes. These two processes are the diffusion of atoms through the grain boundaries and migration of atoms of one

phase through the grain volume of the other phase.

The microstructure evolution of two-phase materials is preferred in polycrystalline materials such as ceramics and metallic alloys. The change of the polycrystalline structure is governed by the organization of the grain boundary set up, the coordination of the grains, and the diffusion mechanism which controls the grain growth.

The variation of grain radius R with time in the existence of different diffusion mechanisms can be expressed as follows [1],

$$\frac{\mathrm{d}R}{\mathrm{d}t} = \frac{D_n a^{n-3}}{R^{n-2}}\left(\Delta - \frac{\alpha}{R}\right), \quad n \geq 2 \tag{1}$$

where a is the lattice constant, R is the grain radius, t is the time, Δ is the system supersaturating, $\alpha = 2\sigma v_a c_0 / k_b T$, σ is the surface tension, v_a is the atomic volume, c_0 is the equilibrium concentration, k_b is the Boltzmann constant, T is the temperature, and the factor $D_n a^{n-3}$ characterizes the diffusion mechanism. It can be observed from Equation (1) that growth rates for several diffusion mechanisms can be renowned by their coefficient and the exponent of $1/R$. When $n = 2$, Equation (1) produces the expression for the growth rate in the case of grain growth controlled by interfacial energy [2]. When $n = 3$, Equation (1) produces the expression for the growth rate in the case of Ostwald ripening controlled by volume diffusion [3]. When $n = 4$, Equation (1) produces the expression for the growth rate in the case of Ostwald ripening controlled by grain boundary diffusion [4].

The hypothetical origin of Ostwald ripening and polycrystalline grain growth was first considered by Lifshitz, Sloyzov and Wagner [3] [5]. In specific, in these formative works, the linking between the grain size distribution function and the leading growth law by the continuity equation has been recognized. These and following Ostwald ripening theory comprising the additions to higher volume fractions of the growing phase can be found in previous works [6] [7].

The average number of sides $s(x)$ as a function of x was considered in earlier reviews [8] [9] [10]. Mullins, [8] exhibited that the von Neumann-Mullins rule helps to find the grain size distribution function $U(x)$ from the topological size function $s(x)$ in terms of x. Furthermore, he proved that $s(x)$ has a nonlinear relation with x.

Computer simulation methods have been developed to study the microstructural and topological evolution of polycrystalline materials e.g., in [11]-[17]. Anderson *et al.* [11] employed three dimensional Monte Carlo Potts model to simulate grain growth. The simulation results are used to analyze grain size distribution, topological distribution and grain size-topology relationships. Their results were consistent with experimental observations.

Zöllner and Streitenberger [18] used Monte Carlo simulations for one phase system to study the relation between the number of sides of each individual grains and the relative grain size of the encircled grain.

El-Khozondar [19] considered grain growth in solid-liquid materials for a

wide range of volume fractions of the solid phase. It was shown that the grain topology distribution is time invariant.

In this paper, we will introduce the application of Monte Carlo Potts model to simulate the microstructure evolution for different diffusion mechanisms in two-phase polycrystalline materials in the self-similar growth regime. The self-similar growth regime happens when the microstructure shows a constant growth in size. This kind of growth is described by time invariant of the scaled size distribution $f(x)$, where x is the relative grain size defined as $x = R/\langle R\rangle$ and the distribution topology $f(s)$, where s is the number of grain sides. The diffusion mechanisms which considered are grain boundary migration in one phase system, grain boundary diffusions and volume diffusion in two-phase system. The focus of this work is on two-phase polycrystalline materials while the previous work was concerned about one-phase system [18] and solid-liquid materials [19]. The simulation results for two-phase system will be compared to the simulations for one-phase system. In the following section, the topological size relationship function will be derived. In Section 3, the numerical model will be described. The simulation results will be presented in Section 4 followed by the conclusion in Section 5.

2. Number of Sides per Grain and Grain Size Relationship

In the self-similar regime the average growth law can be written as [8]

$$\dot{R} = \left\langle \dot{R} \right\rangle \cdot U(x) \tag{2}$$

where $U(x)$ is a probability distribution of the relative grain size x and can be expressed as follows [9].

$$U(x) = -\frac{2(x - x_0)}{ax} + x \tag{3}$$

and can be rewritten as

$$U(x) = \frac{1}{x}\left(\left(1 - \frac{2}{a}\right)x^2 + \frac{4xx_0}{a} - \frac{2}{a}x_0^2\right) \tag{4}$$

The von Neumann-Mullins rule gives the probability distribution in the next equation

$$U(x) = \frac{k}{6x}(s(x) - 6) \tag{5}$$

where $s(x)$ is the topological size relationship function signifying the average number of sides of grains of size R. Solving (4) and (5) together, we get

$$s(x) = b_0 x^2 + b_1 x + b_2$$

where

$$b_0 = \frac{6}{k}\left(1 - \frac{2}{a}\right),\quad b_1 = \frac{24x_0}{ak},\quad b_2 = 6\left(1 - \frac{2x_0^2}{ak}\right).$$

It can be seen that the number of sides of the individual grains varies non-linearly

with the relative grain size in the self-similar regime.

3. The Numerical Model

The Monte Carlo Potts model for two-phase polycrystalline materials has been used to implement the simulations. This model has shown to be successful for simulating microstructural evolution in one, two and three phase systems [20]-[32].

The microstructure of a two-phase polycrystalline material is embodied by a 400×400 square array of lattice sites. Every lattice site is given a specific number varies between 1 and Q which resembles to its orientation. The sign of Q defines the phase at which the site is embedded and $Q = 100$ in all the simulations. All sites are given positive numbers in phase A and negative numbers in phase B.

The initial microstructure was produced by giving each site a random number with the chosen volume fraction of both phases. In two-phase polycrystalline materials, there are two grain boundary energies (*Eaa* and *Ebb*) and there are interfacial boundary energies between phase A and Phase B (*Eab*). The total energy is calculated by using the following equation

$$E = \frac{1}{2}\sum_{i=1}^{N}\sum_{j=1}^{8}\left(\sigma_{ii} + \sigma_{jj} + \sigma_{ij}\right)\left[1 - \delta\left(q_i, q_j\right)\right] \tag{6}$$

where the exterior summation contains all sites i, the internal summation includes the 8 nearest neighbors of site i, δ is the Kronecker delta function and σ_{ii}, σ_{jj} and σ_{ij} relates to the *Eaa*, *Ebb* and *Eab* interfacial energies correspondingly.

Ostwald ripening is simulated as follows. A site and its orientation are selected randomly. Then, the orientation of the picked site is flipped to the new arrangement if the total energy of the system is less than or equal to zero. If the total energy increased, an arbitrary number between 0 and 1 is picked. The new arrangement will be accepted if the arbitrary number is less than or equal to $exp(-\Delta E/k_b T)$ where ΔE is the total energy, k_b is the Boltzman constant and T is the temperature. The temperature has the value of $T = 0.7$ in the case of Ostwald ripening is controlled by grain boundary diffusion. While $T = 1.3$ when Ostwald ripening is controlled by volume diffusion. Time is increased by $1/N$ Monte Carlo steps (MCS) after each attempted orientation variation, where N is the entire number of sites.

4. Topological Features Simulation Results

The development of grain structure of the two-phase polycrystalline material is determined by the interfacial energies *Eaa*, *Ebb* and *Eab*.

The grains of phase A and phase B have the same microstructural properties since A-A and B-B grain boundary energies are equal. Therefore, when *Eaa* = *Ebb*, the only factor which impacts grain structure and distribution is the A-B interfacial energy *Eab*. In the process of Ostwald ripening driven by grain boundary diffusion, the values of the interfacial energies are: *Eaa* = 1, *Ebb* = 1 and *Eab* = 1. When the process of Ostwald ripening controlled by volume diffusion, the

values of the interfacial energies are: *Eaa* = 2.5, *Ebb* = 2.5 and *Eab* = 1. The volume fraction for both phases varies between 20%*B* - 50%*B* and 50%*A* - 80%*A*. The grain growth in one phase system is simulated by switching the value of the volume fraction for phase *B* to zero (0%*B*).

4.1. Evolution of the Average Number of Sides

The dependence of the average number of sides, $\langle s \rangle$, on time is plotted in Figure 1 through Ostwald ripening for different volume fractions of both phases. In Figure 1(a) Ostwald ripening is driven by grain boundary diffusion while in Figure 1(b) Ostwald ripening is driven by volume diffusion. It can be noticed from Figure 1(a) and Figure 1(b) that the average number of sides for phase *A*, $\langle s_A \rangle$, increased whereas the average number of sides for phase *B*, $\langle s_B \rangle$, decreased in the 20%*B* - 80%*A*, 30%*B* - 70%*A*, 40%*B* - 60%*A* and 50%*B* - 50%*A* two-phase polycrystalline materials.

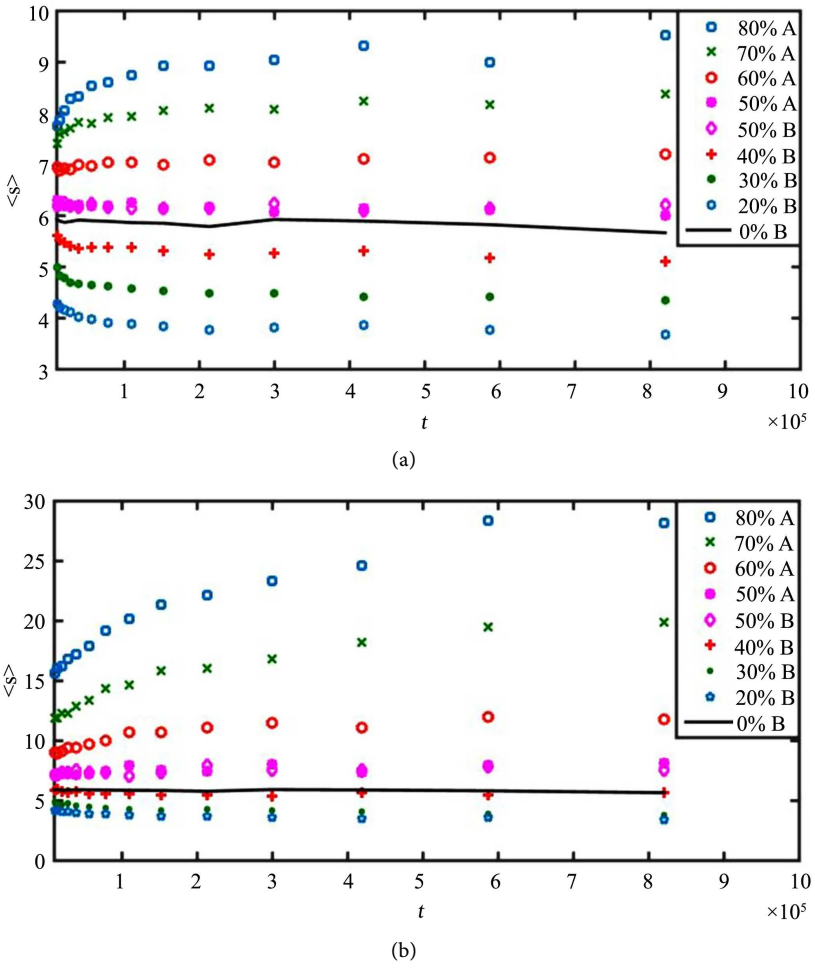

Figure 1. The mean number of sides $\langle s \rangle$ as a function of time, during Ostwald ripening in two-phase systems for different volume fractions. The volume fraction of both phases differs between 20%*B* - 50%*B* and 50%*A* - 80%*A* as specified. The case 0%*B* represents grain growth in one phase system. (a) Ostwald ripening via grain boundary diffusion; (b) Ostwald ripening via volume diffusion.

In Ostwald ripening driven by grain boundary diffusion, the average numbers of sides for phase B, $\langle s_B \rangle$, are 3.7, 4.5, 5.4 and 6.2 for the volume fractions 20%, 30%, 40% and 50% correspondingly. Moreover, the average numbers of sides for phases A, $\langle s_A \rangle$, are 6.2, 7.2, 8.1 and 9.1 for the volume fractions 50%, 60%, 70% and 80% correspondingly.

In Ostwald ripening driven by volume diffusion, the average numbers of sides for phase B, $\langle s_B \rangle$, are 3.6, 3.9, 5.5 and 7.9 for the volume fractions 20%, 30%, 40% and 50% correspondingly. Moreover, the average numbers of sides for phases A, $\langle s_A \rangle$, are 7.9, 11.8, 19.7 and 28.2 for the volume fractions 50%, 60%, 70% and 80% correspondingly.

While the average number of sides for the overall grain structure in one-phase polycrystalline materials has the value of $\langle s \rangle = 6$. It can be seen that the effect of volume fraction on the mean number of sides for both phases is evident in the simulations for two-phase systems.

4.2. The Grain Topology Distributions

The distribution of the number of sides, $f(s)$, for individual grain is plotted in Figure 2 and Figure 3 at five different time steps (7379 MCS, 10331 MCS, 14463 MCS, 20248 MCS and 28348 MCS). The grain topology distributions observed in the two-phase simulated microstructure, which evolves by Ostwald ripening for a wide range of volume fractions. The volumes fractions of the simulated microstructure differ between 20%B - 80%A, 30%B - 70%A, 40%B - 60%A and 50%B - 50%A for both phases. For Ostwald ripening driven by grain boundary diffusion, the grain topology distributions are presented in Figure 2. Whereas Figure 3 displays the grain topology distributions for Ostwald ripening controlled by volume diffusion. It can be seen from Figure 2 and Figure 3 that the frequency of the number of sides per grain raises rapidly for a small number of sides and it crests at a definite value and then drops more gradually for all cases; furthermore grain topology distributions, $f(s)$, is time invariant in the self-similar regime.

The grain topology distribution has a maximum value nearby $s = 5$ for one-phase simulations represented by 0%B. For simulation of Ostwald ripening driven by grain boundary diffusion, the grain topology distribution of the phase B in the 20%B - 80%A, 30%B - 70%A, 40%B - 60%A and 50%B - 50%A two-phase systems have maximum values near $s = 4$, $s = 5$, $s = 5$ and $s = 6$. While, the grain topology distribution of the phase A in the 20%B - 80%A, 30%B - 70%A, 40%B - 60%A and 50%B - 50%A two-phase systems are peaked nearby $s = 7$, $s = 7$, $s = 6$ and $s = 6$; moreover, the grain topology distribution is narrower for smaller volume fractions and broader for larger volume fractions.

For simulation of Ostwald ripening controlled by volume diffusion, the grain topology distribution of the phase B in the 20%B - 80%A, 30%B - 70%A, 40%B - 60%A and 50%B - 50%A two-phase systems are peaked near $s = 4$, $s = 4$, $s = 4$ and $s = 7$. Whereas, the grain topology distribution of the phase A in the 20%B - 80%A, 30%B - 70%A, 40%B - 60%A and 50%B - 50%A two-phase systems have maximum values around $s = 16$, $s = 11$, $s = 9$ and $s = 7$; additionally, the grain

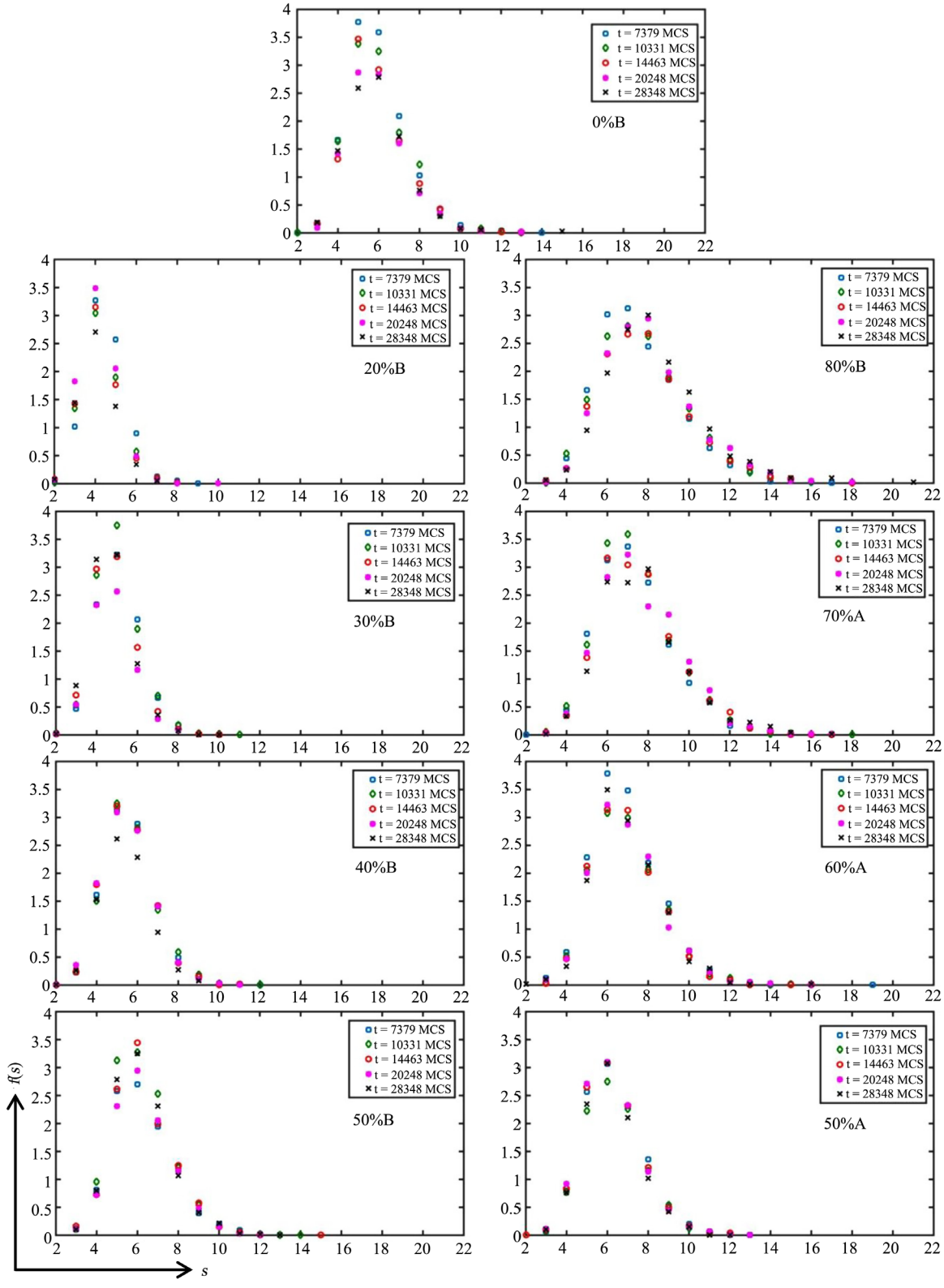

Figure 2. The grain topology distributions during Ostwald ripening in two phase systems for various volume fractions. Ostwald ripening is driven by grain boundary diffusion. The volume fraction varies between 20%B - 50%B and 50%A - 80%A for both phases as specified. The case 0%B represents grain growth in one phase system. The data is taken for different five time steps as indicated.

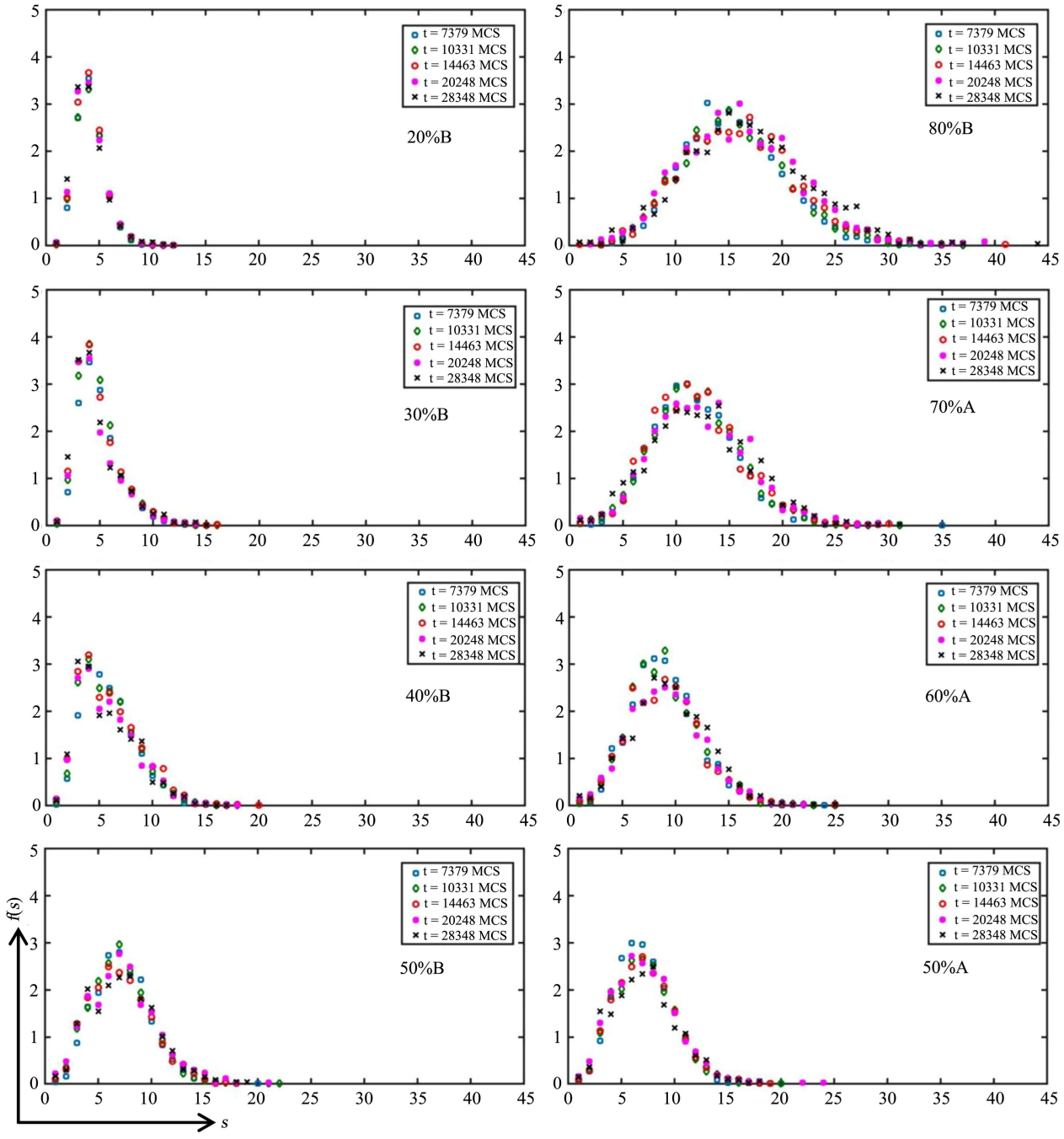

Figure 3. The grain topology distributions during Ostwald ripening in two phase systems for various volume fractions. Ostwald ripening is driven by volume diffusion. The volume fraction varies between 20%B - 50%B and 50%A - 80%A for both phases as specified. The data is taken for different five time steps as indicated.

topology distribution is narrower for smaller volume fractions and broader for larger volume fractions.

It can be noticed that for different diffusion mechanisms, the grain topology distribution is asymmetric. In addition, it skewed to smaller values of s for smaller volume fractions as well as it skewed to larger values of s for higher volume fractions.

4.3. Grain Size-Number of Sides per Grain Topology

The topological size relation function, which expresses the number of sides per grain s in terms of the relative grain size x is a main topological property of the microstructure.

Figure 4 displays the topological size relation function for grain growth in one phase. This relation is considered for five time steps: 7379 MCS, 10331 MCS, 14463 MCS, 20248 MCS and 28348 MCS. It can be seen from Figure 4 that the

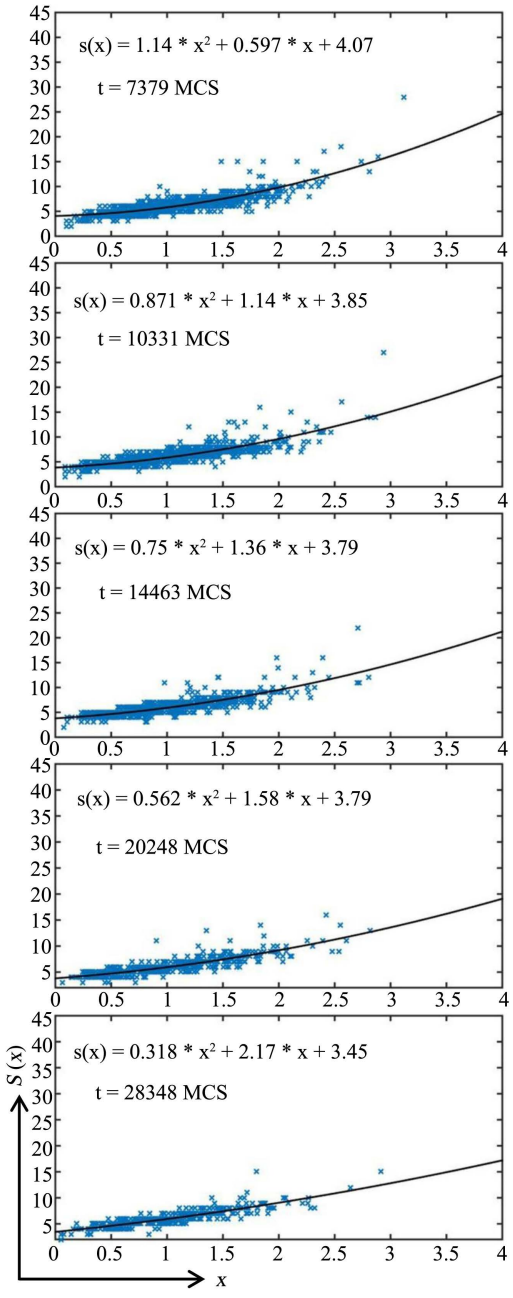

Figure 4. Number of edges as a function of relative grain size for all grains of an ensemble (crosses) together with quadratic fit (solid line). The data is taken from simulation of grain growth in one phase for different five time steps as indicated.

number of sides per grain varies none linearly with the relative grain size in the self-similar regime. The relation can be estimated by a quadratic function. This is in agreement with experimental remarks [32] and other computer simulations [25] [26].

The topological size function is exhibited in **Figures 5-12** at five different time steps (7379 MCS, 10331 MCS, 14463 MCS, 20248 MCS and 28348 MCS) for different diffusion mechanisms over a wide range of volume fractions. The volumes fractions of the simulated microstructure vary between 20%B - 80%A, 30%B - 70%A, 40%B - 60%A and 50%B - 50%A for both phases. The topological size function considered in the two-phase simulated microstructure, which grows by Ostwald ripening. For Ostwald ripening driven by grain boundary diffusion, the topological size function is illustrated in **Figures 5-8**. Whereas **Figures 9-12** show the grain topology distributions for Ostwald ripening controlled by volume diffusion. It can be noticed that the number of sides for individual grain changes none linearly with the relative grain size in the self-similar regime. Furthermore, topological size function in two-phase microstructure can be assessed by a quadratic function. This is similar to the relation obtained in one-phase microstructure and in agreement previous experimental works and computer simulations [25] [26] [32].

According to the previous sections, the main results in the two-phase polycrystalline materials for different diffusion mechanisms over a wide range of volume fractions are summarized in the following points:

- The mean number of sides increased for the major phase while the average number of sides for the minor phase decreased.
- The grain topology distribution is asymmetric and tilted to smaller values of s for smaller volume fractions and to larger values of s for higher volume fractions over a broad variety of volume fractions.
- The number of sides for individual grain changes none linearly with the relative grain size in the self-similar regime and can be expressed by a quadratic function.

5. Conclusion

Computer simulation technique based on Monte Carlo Potts model has been developed to predict the main topological features of the microstructure in two-phase polycrystalline materials. The simulated microstructures were developed by different diffusion mechanisms such as grain boundary migration, grain boundary diffusion and volume diffusion. The topological features were analyzed over a wide range of volume fractions. The key findings for different diffusion mechanisms in two phase system at different volume fractions are: the mean number of sides varies as the volume fraction changes, the grain topology distribution is time invariant in the self-similar growth regime and the number of sides per grain of the individual grains depends none linearly on the relative grain size. The results for one-phase system are consistent with experimental works [32] and computer simulations [25] [26]. Moreover, the results in two-phase

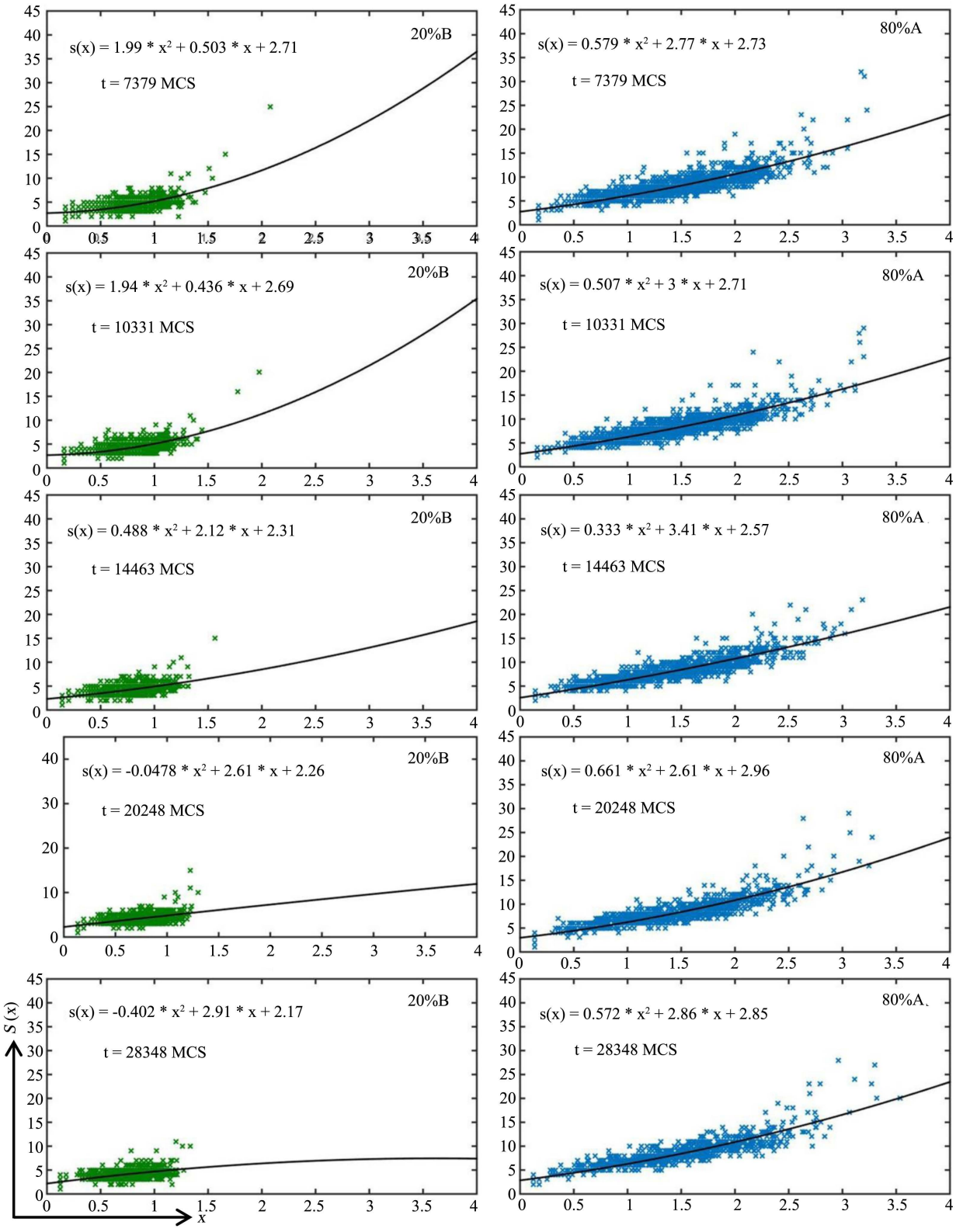

Figure 5. Number of edges as a function of relative grain size for all grains of an ensemble (crosses) together with quadratic fit (solid line). The data is taken from simulation of Ostwald ripening in two-phase systems for different five time steps as indicated. Ostwald ripening is driven by grain boundary diffusion. The volume fraction is 20% for phase *B* and 80% for phase *A* as specified. The blue color represents phase *A* and the green color represents phase *B*.

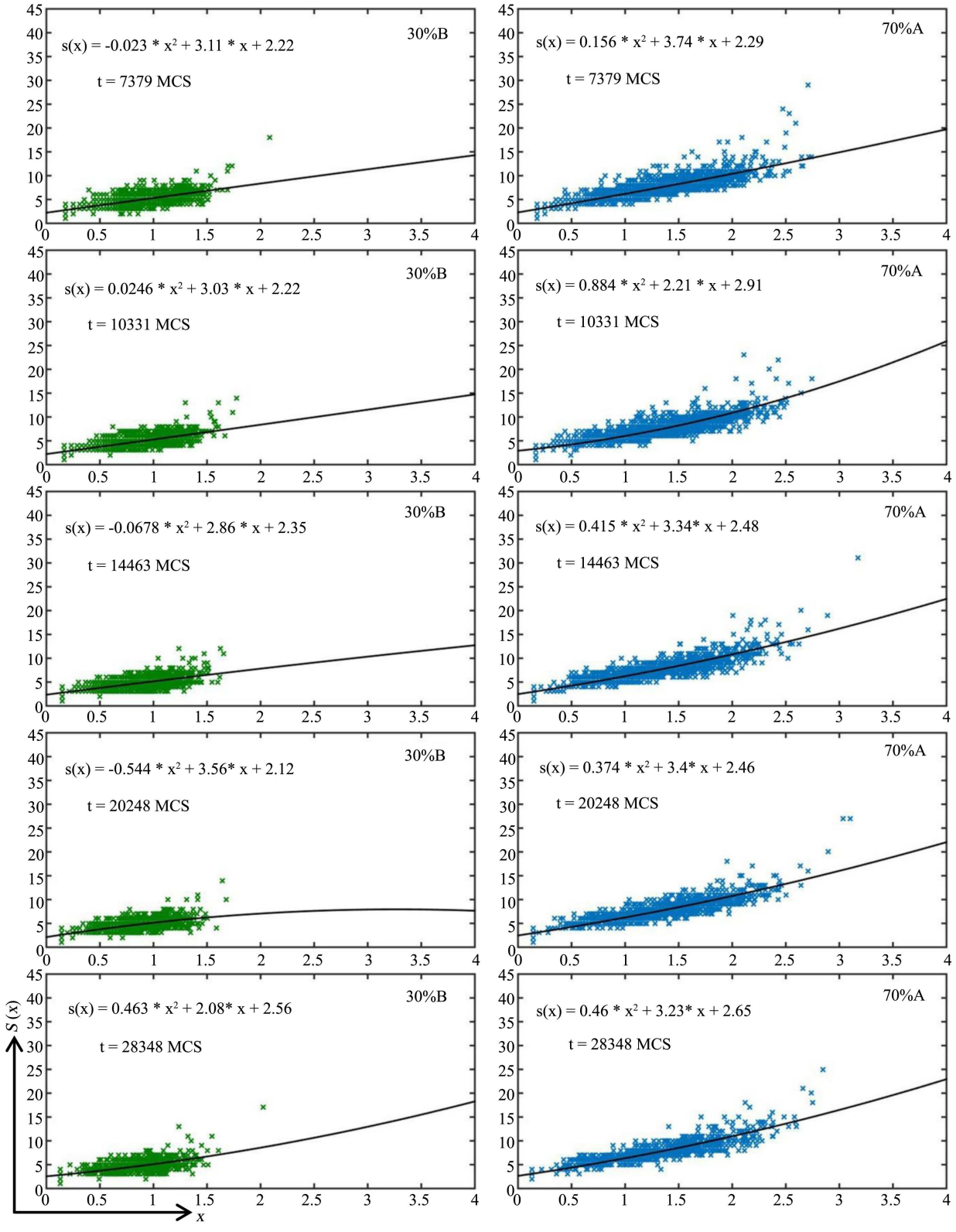

Figure 6. Number of edges as a function of relative grain size for all grains of an ensemble (crosses) together with quadratic fit (solid line). The data is taken from simulation of Ostwald ripening in two-phase systems for different five time steps as indicated. Ostwald ripening is driven by grain boundary diffusion. The volume fraction is 30% for phase *B* and 70% for phase *A* as specified. The blue color represents phase *A* and the green color represents phase *B*.

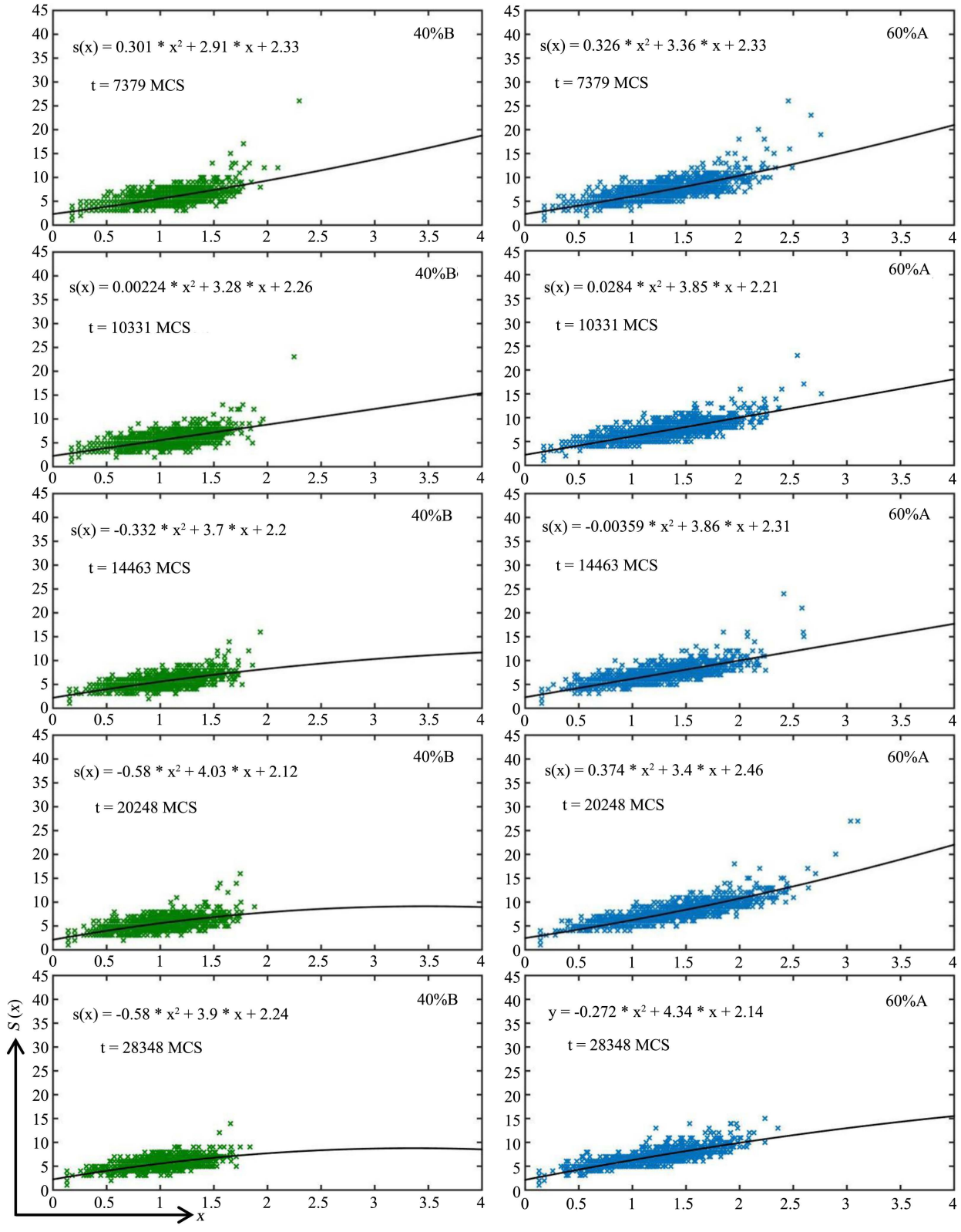

Figure 7. Number of edges as a function of relative grain size for all grains of an ensemble (crosses) together with quadratic fit (solid line). The data is taken from simulation of Ostwald ripening in two-phase systems for different five time steps as indicated. Ostwald ripening is driven by grain boundary diffusion. The volume fraction is 40% for phase *B* and 60% for phase *A* as specified. The blue color represents phase *A* and the green color represents phase *B*.

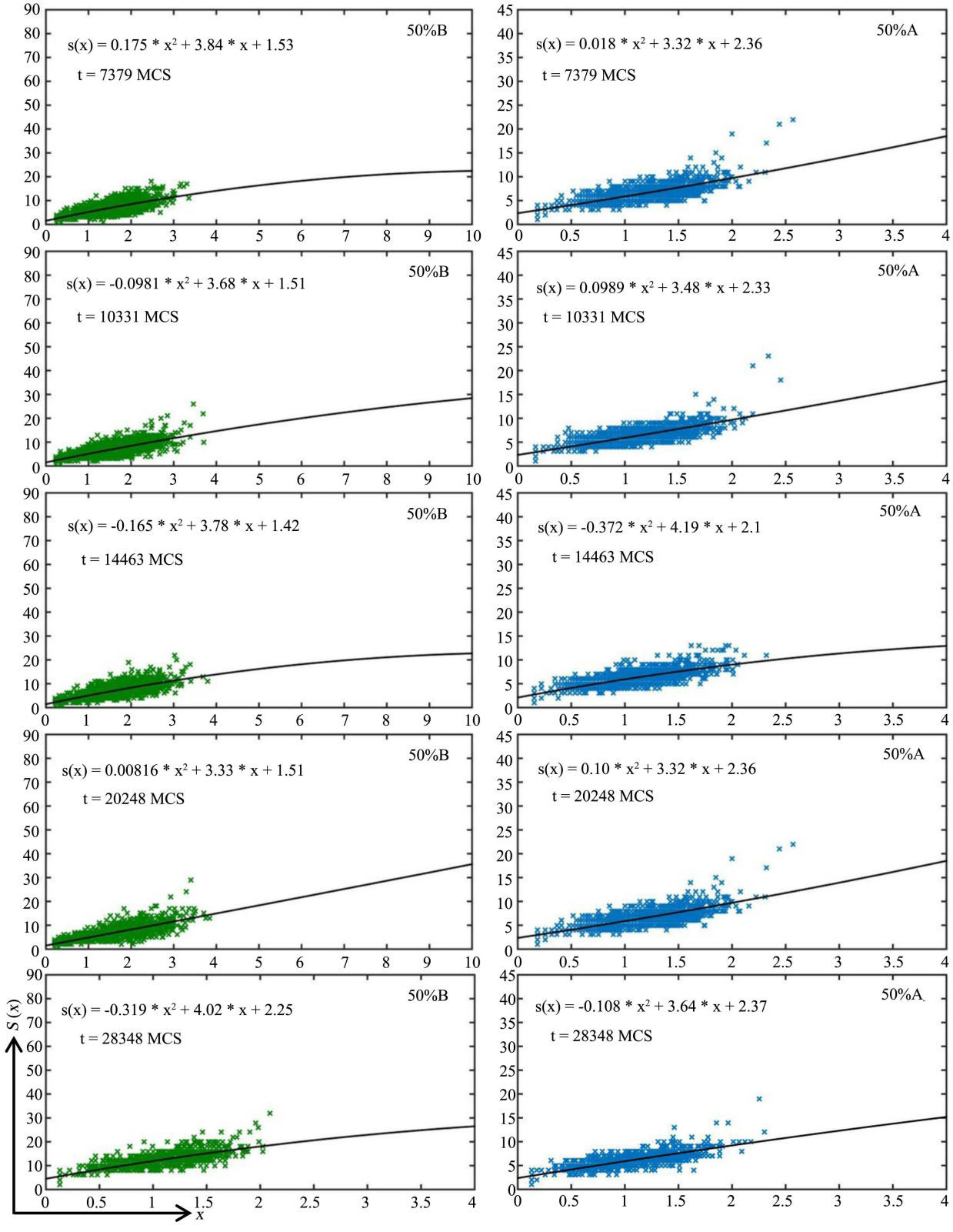

Figure 8. Number of edges as a function of relative grain size for all grains of an ensemble (crosses) together with quadratic fit (solid line). The data is taken from simulation of Ostwald ripening in two-phase systems for different five time steps as indicated. Ostwald ripening is driven by grain boundary diffusion. The volume fraction is 50% for phase *B* and 50% for phase *A* as specified. The blue color represents phase *A* and the green color represents phase *B*.

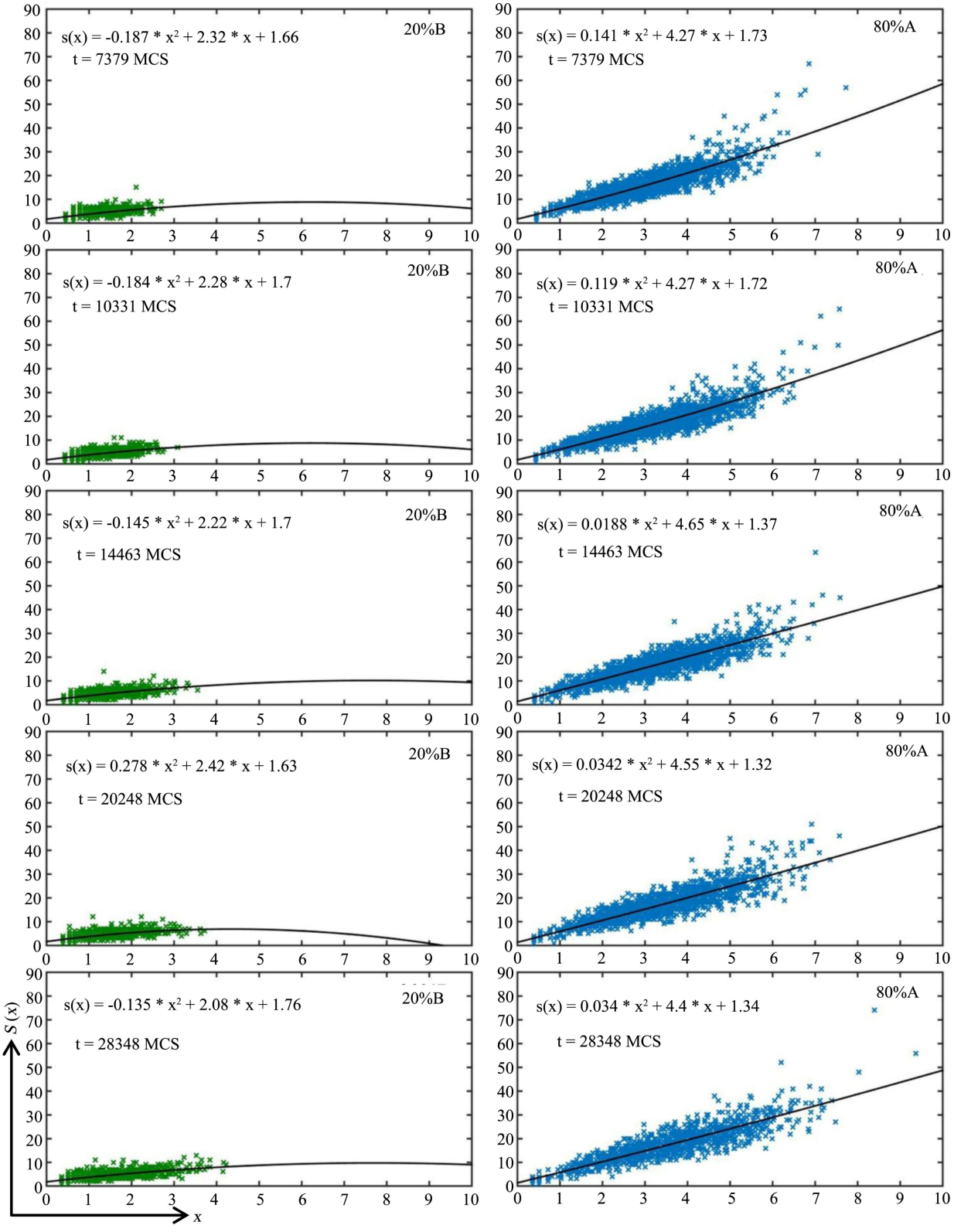

Figure 9. Number of edges as a function of relative grain size for all grains of an ensemble together with quadratic fit. The data is taken from simulation of Ostwald ripening in two-phase systems for different five time steps as indicated. Ostwald ripening is driven by volume diffusion. The volume fraction is 20% for phase *B* and 80% for phase *A* as specified. The blue color represents phase *A* and the green color represents phase *B*.

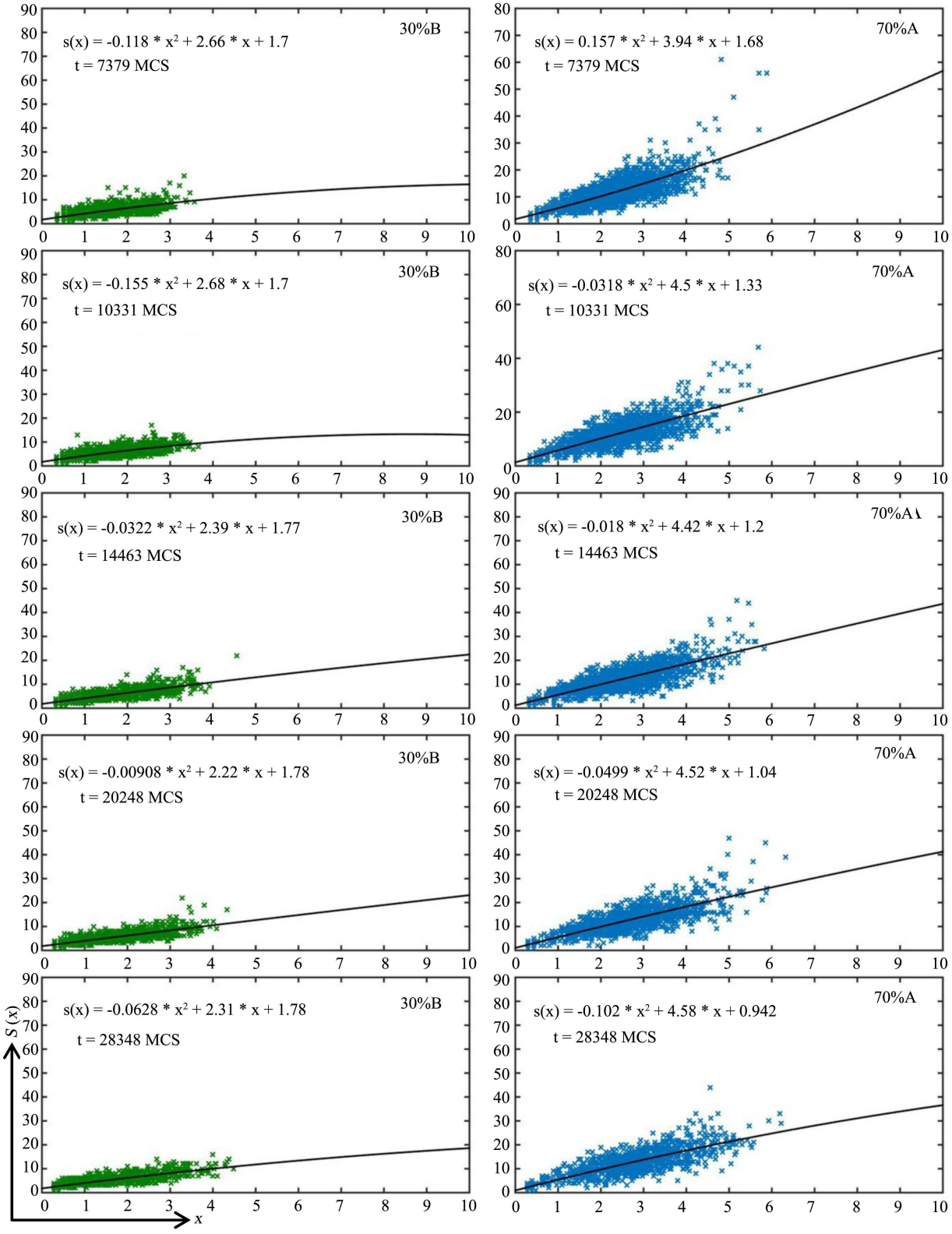

Figure 10. Number of edges as a function of relative grain size for all grains of an ensemble together with quadratic fit. The data is taken from simulation of Ostwald ripening in two-phase systems for different five time steps as indicated. Ostwald ripening is driven by volume diffusion. The volume fraction is 30% for phase *B* and 70% for phase *A* as specified. The blue color represents phase *A* and the green color represents phase *B*.

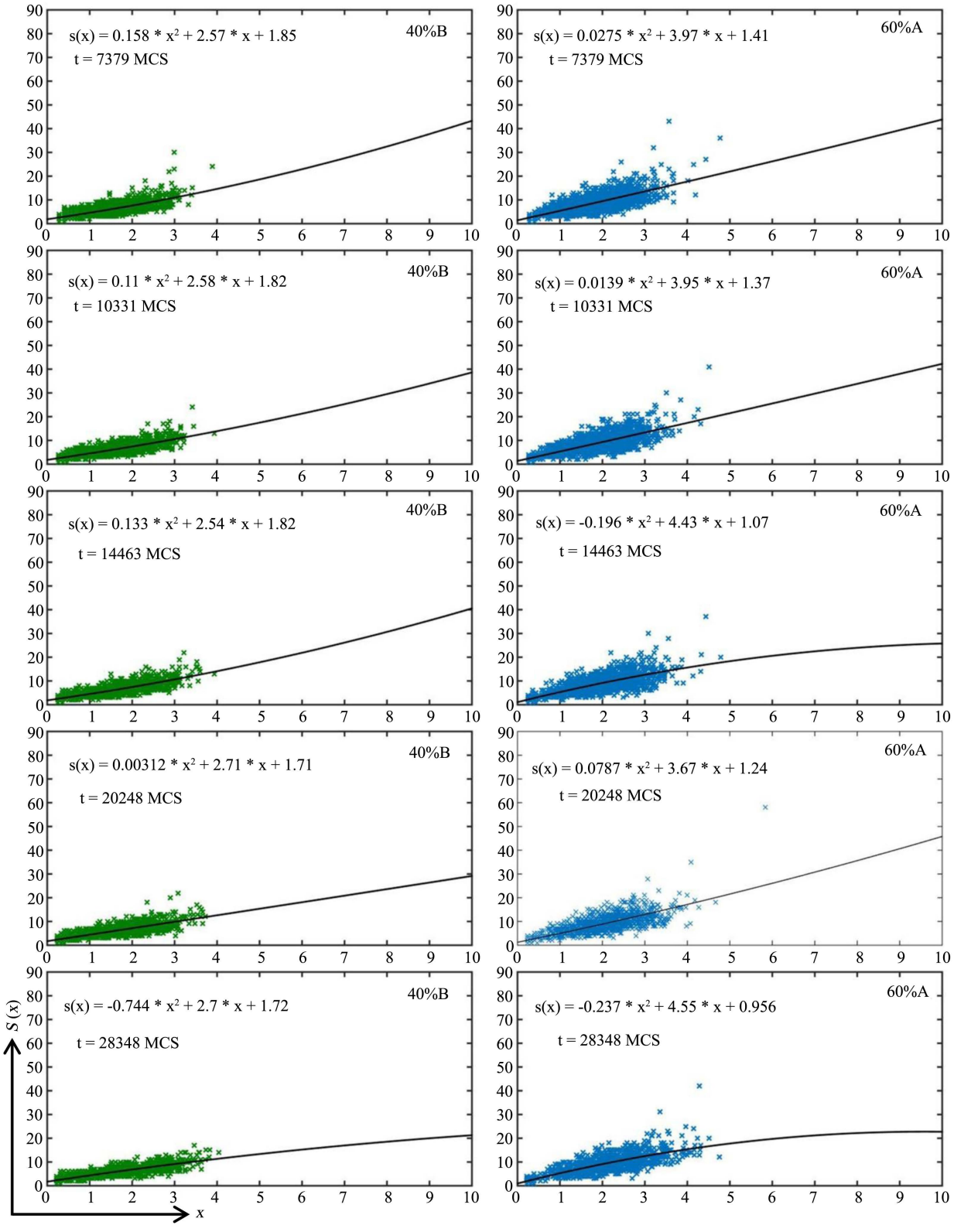

Figure 11. Number of edges as a function of relative grain size for all grains of an ensemble together with quadratic fit. The data is taken from simulation of Ostwald ripening in two-phase systems for different five time steps as indicated. Ostwald ripening is driven by volume diffusion. The volume fraction is 40% for phase *B* and 60% for phase *A* as specified. The blue color represents phase *A* and the green color represents phase *B*.

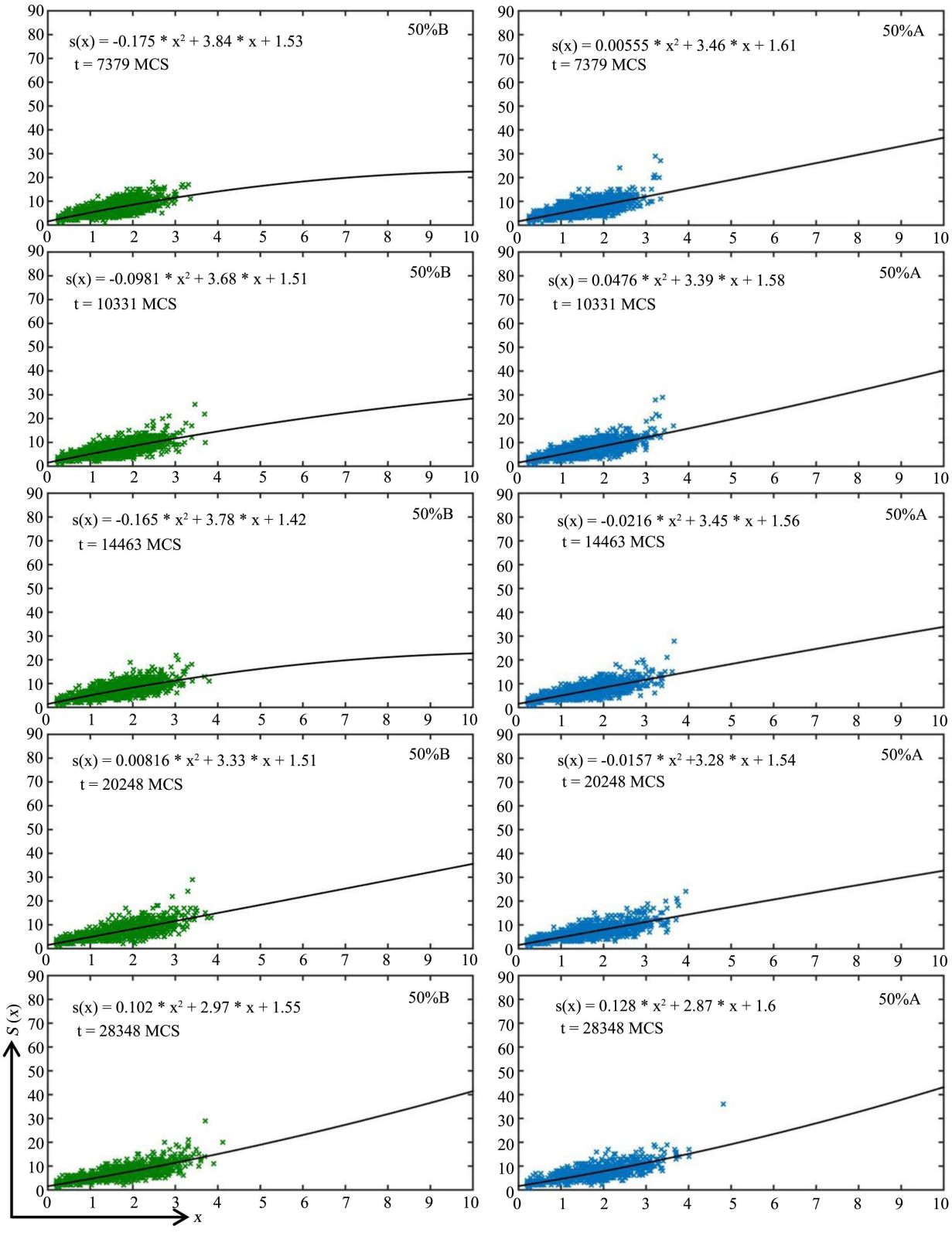

Figure 12. Number of edges as a function of relative grain size for all grains of an ensemble together with quadratic fit. The data is taken from simulation of Ostwald ripening in two-phase systems for different five time steps as indicated. Ostwald ripening is driven by volume diffusion. The volume fraction is 50% for phase *B* and 50% for phase *A* as specified. The blue color represents phase *A* and the green color represents phase *B*.

system have similar behavior as one-phase system. It is recommended to do experimental work in two-phase system to verify the simulation results.

Conflicts of Interest

The author declares no conflicts of interest regarding the publication of this paper.

References

[1] Slezov, V.V., Sagalovich, V.V. and Tanatarov, L.V. (1978) Theory of Diffusive Decomposition of Supersaturated Solid Solution under the Condition of Simultaneous Operation of Several Mass-Transfer Mechanisms. *Journal of Physics and Chemistry of Solids*, **39**, 705-709. https://doi.org/10.1016/0022-3697(78)90002-1

[2] Hillert, M. (1965) On the Theory of Normal and Abnormal Grain Growth. *Acta Metallurgica*, **13**, 227-238. https://doi.org/10.1016/0001-6160(65)90200-2

[3] Lifshitz, I.M. and Slyozov, V.V. (1961) The Kinetics of Precipitation from Supersaturated Solid Solutions. *Journal of Physics and Chemistry of Solids*, **19**, 35-50. https://doi.org/10.1016/0022-3697(61)90054-3

[4] Ardell, A.J. (1972) On the Coarsening of Grain Boundary Precipitates. *Acta Metallurgica*, **20**, 601-609. https://doi.org/10.1016/0001-6160(72)90015-6

[5] Wagner, C. (1961) Theorie der Alterung von Niderschlagen durch Umlösen. *Electrochem*, **65**, 581-591.

[6] Baldan, A. (2002) Review Progress in Ostwald Ripening Theories and Their Applications to Nickel-Base Superalloys Part I: Ostwald Ripening Theories. *Journal of Materials Science*, **37**, 2171-2202.

[7] Streitenberger, P. (2013) Analytical Description of Phase Coarsening at High Volume Fractions. *Acta Materialia*, **61**, 5026-5035. https://doi.org/10.1016/j.actamat.2013.04.042

[8] Mullins, W.W. (1998) Grain Growth of Uniform Boundaries with Scaling. *Acta Materialia*, **46**, 6219-6226. https://doi.org/10.1016/S1359-6454(98)00259-6

[9] Zöllner, D. and Streitenberger, P. (2006) Three-Dimensional Normal Grain Growth: Monte Carlo Potts Model Simulation and Analytical Mean Field Theory. *Scripta Materialia*, **54**, 1697-1702. https://doi.org/10.1016/j.scriptamat.2005.12.042

[10] Glicksman, M.E. (2005) Analysis of 3-D Network Structures. *Philosophical Magazine*, **85**, 3-31. https://doi.org/10.1080/14786430412331329892

[11] Anderson, M.P., Grest, S. and Srolovitz, D.J. (1989) Computer Simulation of Normal Grain Growth in Three Dimensions. *Philosophical Magazine*, **59**, 293-329. https://doi.org/10.1080/13642818908220181

[12] Fan, D. and Chen, L.-Q. (1997) Topological Evolution during Coupled Grain Growth and Ostwald Ripening in Volume-Conserved 2-D Two-Phase Polycrystals. *Acta Metallurgica*, **45**, 4145-4154. https://doi.org/10.1016/S1359-6454(97)00101-8

[13] Fan, D., Geng, C. and Chen, L.-Q. (1996) Computer Simulation of Topological Evolution in 2-D Grain Growth Using a Continuum Diffuse-Interface Field Model. *Acta Metallurgica*, **45**, 1115-1126. https://doi.org/10.1016/S1359-6454(96)00221-2

[14] Fan, D. and Chen, L.-Q. (1997b) Computer Simulation of Grain Growth and Ostwald Ripening in Alumina-Zirconia Two-Phase Composite. *Journal of the American Ceramic Society*, **80**, 1773-1780. https://doi.org/10.1111/j.1151-2916.1997.tb03051.x

[15] Fan, D., Chen, L.-Q. and Chen, S.P.P. (1998) Numerical Simulation of Zener Pinning with Growing Second-Phase Particles. *Journal of the American Ceramic Society*, **81**, 526-532. https://doi.org/10.1111/j.1151-2916.1998.tb02370.x

[16] Chen, L. and Fan, D. (1996) Computer Simulation Model for Coupled Grain Growth and Ostwald Ripening-Applications to Al_2O_3-ZrO_2 Two-Phase Systems. *Journal of the American Ceramic Society*, **79**, 1163-1168. https://doi.org/10.1111/j.1151-2916.1996.tb08568.x

[17] Poulsen, S.O., Voorhees, P.W. and Lauridsen, E.M. (2013) Three-Dimensional Simulations of Microstructural Evolution in Polycrystalline Dual-Phase Materials with Constant Volume Fractions. *Acta Materialia*, **61**, 1220-1228. https://doi.org/10.1016/j.actamat.2012.10.032

[18] Zöllner, D. and Streitenberger, P. (2008) Monte Carlo Simulation of Normal Grain Growth in Three Dimensions. *Materials Science Forum*, **567-568**, 81-84. https://doi.org/10.4028/www.scientific.net/MSF.567-568.81

[19] El-Khozondar, R.J. and El-Khozondar, H.J. (2016) Grain Size Distribution and Topological Correlations during Ostwald Ripening: Monte Carlo Potts Model Simulation. *Al-Aqsa University Journal* (*Natural Sciences Series*), **20**, 44-60. https://doi.org/10.12816/0033303

[20] Holm, E.A., Srolovitz, D.J. and Chan, J.W. (1993) Microstructural Evolution in Two-Dimensional Two-Phase Polycrystals. *Acta Metallurgica et Materialia*, **41**, 1119-1136. https://doi.org/10.1016/0956-7151(93)90160-T

[21] El-Khozondar, R., El-Khozondar, H., Gottstein, G. and Rollett, A.D. (2006) Microstructural Simulation of Grain Growth in Two-Phase Polycrystalline Materials. *Egyptian Journal of Solids*, **29**, 35-47.

[22] Solomatov, V.S., El-Khozondar, R. and Tikare, V. (2002) Grain Size in the Lower Mantle: Constraints from Numerical Modeling of Grain Growth in Two-Phase Systems. *Physics of the Earth and Planetary Interiors*, **129**, 265-282. https://doi.org/10.1016/S0031-9201(01)00295-3

[23] Grest, G.S., Srolovitz, D.J. and Anderson, M.P. (1988) Domain-Growth Kinetics for the *Q*-State Potts Model in Two and Three Dimensions. *Physical Review B*, **38**, 4752-4760. https://doi.org/10.1103/PhysRevB.38.4752

[24] Anderson, M.P., Srolovitz, D.J., Grest, G.S. and Sahni, P.S. (1984) Computer Simulation of Grain Growth. I. Kinetics. *Acta Metallurgica*, **32**, 783-791. https://doi.org/10.1016/0001-6160(84)90151-2

[25] El-Khozondar, R. and El-Khozondar, H. (2015) Monte Carlo Potts Simulation of Grain Growth of Solid Grains Dispersed in a Liquid Matrix. *Journal of Engineering Research* and Technology, **2**, 7-14.

[26] El-Khozondar, R., Zöllner, D. and Kassner, K. (2014) Numerical Simulation of Grain Size Distribution in Two-Phase Polycrystalline Materials. *International Journal of Materials Science and Applications*, **3**, 381-390. https://doi.org/10.11648/j.ijmsa.20140306.26

[27] Zöllner, D. and Streitenberger, P. (2004) Computer Simulations and Statistical Theory of Normal Grain Growth in Two and Three Dimensions. *Materials Science Forum*, **467-470**, 1129-1136. https://doi.org/10.4028/www.scientific.net/MSF.467-470.1129

[28] El-Khozondar, R. and El-Khozondar, H. (2009) Numerical Modeling of Microstructural Evolution in Three-Phase Polycrystalline Materials. *The Arabian Journal for Science and Engineering*, **34**, 241-252.

[29] El-Khozondar, R.J. and El-Khozondar, H.J. (2017) Monte Carlo Implementation for

Simulation of Ostwald Ripening via Long Range Diffusion in Two-Phase Solids. *International Journal of Engineering Science Invention*, **6**, 29-37.

[30] Zöllner, D. and Streitenberger, P. (2010) Grain Size Distributions in Normal Grain Growth. *Practical Metallography/ Praktische Metallographie*, **47**, 618-639. https://doi.org/10.3139/147.110100

[31] Tikare, V. and Cawley, J.D. (1998) Numerical Simulation of Grain Growth in Liquid Phase Sintered Materials. II. Study If Isotropic Grain Growth. *Acta Materialia*, **46**, 1343-1356. https://doi.org/10.1016/S1359-6454(97)00269-3

[32] Zhang, C., Suzuki, A., Ishimaru, T. and Enomoto, M. (2004) Characterization of Three-Dimensional Grain Structure in Polycrystalline Iron by Serial Sectioning. *Metallurgical and Materials Transactions A*, **35**, 1927-1933. https://doi.org/10.1007/s11661-004-0141-5